ARMY RESEARCH LABORATORY

Mortar Interior Ballistics: Sensitivity Studies Using IBHVG2 and Progress Toward a Multidimensional Representation

by John R. Schmidt, Michael J. Nusca, and Albert W. Horst

ARL-TR-4838 **June 2009**

NOTICES

Disclaimers

The findings in this report are not to be construed as an official Department of the Army position unless so designated by other authorized documents.

Citation of manufacturer's or trade names does not constitute an official endorsement or approval of the use thereof.

Destroy this report when it is no longer needed. Do not return it to the originator.

Army Research Laboratory
Aberdeen Proving Ground, MD 21005-5066

ARL-TR-4838 **June 2009**

Mortar Interior Ballistics: Sensitivity Studies Using IBHVG2 and Progress Toward a Multidimensional Representation

John R. Schmidt and Michael J. Nusca
Weapons and Materials Research Directorate, ARL

Albert W. Horst
American Systems

REPORT DOCUMENTATION PAGE	Form Approved OMB No. 0704-0188

1. REPORT DATE *(DD-MM-YYYY)*	2. REPORT TYPE	3. DATES COVERED (From - To)
June 2009	Final	May 2006–May 2007

4. TITLE AND SUBTITLE
Mortar Interior Ballistics: Sensitivity Studies Using IBHVG2 and Progress Toward a Multidimensional Representation

5a. CONTRACT NUMBER

5b. GRANT NUMBER

5c. PROGRAM ELEMENT NUMBER

6. AUTHOR(S)
John R. Schmidt, Michael J. Nusca, and Albert W. Horst*

5d. PROJECT NUMBER
622618H8000

5e. TASK NUMBER

5f. WORK UNIT NUMBER

7. PERFORMING ORGANIZATION NAME(S) AND ADDRESS(ES)
U.S. Army Research Laboratory
ATTN: AMSRD-ARL-WM-BD
Aberdeen Proving Ground, MD 21005-5066

8. PERFORMING ORGANIZATION REPORT NUMBER
ARL-TR-4838

9. SPONSORING/MONITORING AGENCY NAME(S) AND ADDRESS(ES)

10. SPONSOR/MONITOR'S ACRONYM(S)

11. SPONSOR/MONITOR'S REPORT NUMBER(S)

12. DISTRIBUTION/AVAILABILITY STATEMENT
Approved for public release; distribution is unlimited.

13. SUPPLEMENTARY NOTES
*American Systems, Aberdeen, MD 21001

14. ABSTRACT
Traditionally, the interior ballistic (IB) modeling of mortars has been difficult to achieve because a mortar projectile contains certain energetic components internal to the tail boom. After ignition, high pressure generated by the igniter causes the canister to burst and release hot gases and burning particles into the larger chamber called the launch tube. Subsequently, any external charges ignite and produce gases which accelerate the projectile. A recent advancement to the IBHVG2 code allows the modeling of this high-low (HILO) configuration. This HILO feature comes with the introduction of two new parameters into the IBHVG2 model, essentially gas-phase and solid-phase discharge coefficients governing flow between the two chambers.
The large-caliber gun community focuses on the impact of seven IB input variables (charge weight, force, propellant diameter, burning rate coefficient and exponent, covolume, and projectile weight) on the peak chamber pressure and projectile exit velocity. A sensitivity study on these input variables was performed on the high and low canister over a small range of the nominal value. The HILO feature was also examined for a 120-mm mortar. Uncertainty associated with the two new free parameters necessitated a wider range of investigation of said parameters.

15. SUBJECT TERMS
interior ballistics, mortar, CFD, two-phase flow, guns

16. SECURITY CLASSIFICATION OF:			17. LIMITATION OF ABSTRACT	18. NUMBER OF PAGES	19a. NAME OF RESPONSIBLE PERSON
a. REPORT	b. ABSTRACT	c. THIS PAGE			John R. Schmidt
Unclassified	Unclassified	Unclassified	UU	38	19b. TELEPHONE NUMBER (*Include area code*) 410-278-5510

Contents

List of Figures

INTENTIONALLY LEFT BLANK.

1. Background

The modern smoothbore U.S. Army mortar (figure 1) is basically a gun tube with a firing pin fixed to the breech end. Muzzle loaded and gravity fed, the mortar round is completely self-contained with a flight body, a payload, a primer, a booster charge of black powder, and an igniter charge contained in a high-pressure canister within the tail boom. The possibility of several modules of a main propellant installed around its tail boom also exists. The number of modules can be varied in order to achieve the desired muzzle velocity which, with the elevation, determines the distance traveled by the mortar round (or zone). Mortars are fired at very steep angles. Once in flight, most modern mortar rounds are fin stabilized. However, there are some mortar rounds which are spin stabilized.

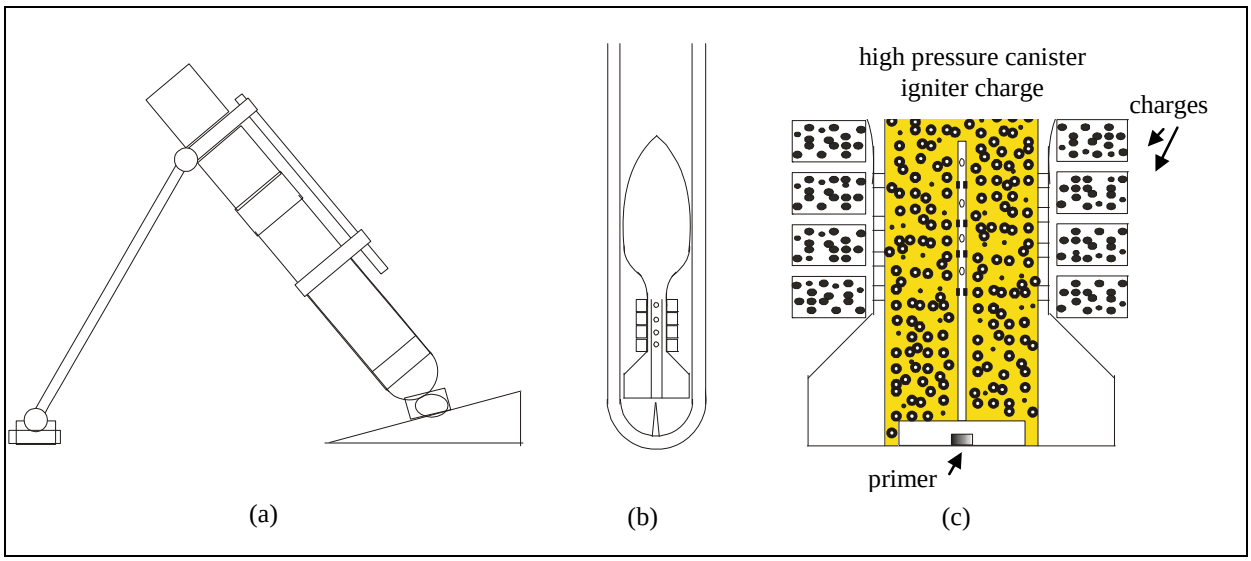

Figure 1. Schematics of a mortar system: (a) footplate and tube, (b) projectile in tube, and (c) cross section of tail boom.

The original designs were reminiscent of the apothecary mixing vessels after which they were named. Mortars are relatively short, having low barrel length-to-diameter ratios when compared to other gun weapons; they are usually less than 20 calibers long. Maneuverable mortars were first used in battle in the late seventeenth century.

Mortars by their very nature are useful in ground maneuvers; history has shown their effectiveness in battles against defilade (dug-in) enemy troops and targets not easily defeated by direct-fire weapons. This is due in no small part to the high angle of attack of mortar weapons. Mortars achieved great acclaim during the trench warfare of WWI after the highly mobile

"Stokes Mortar" was developed, even though they were not very successful against bunkers or tanks. Mortars provide accurate close-in fire for ground troops during battle without the logistics overhead necessary for artillery pieces. Mortar rounds are generally three battle types: high explosive, illumination, and smoke-producing. A plethora of practice rounds used for training also exists. "Smart" mortar rounds have been in production since 1994. The U.S. Army is developing a precision-guided mortar munition and has a vested interest in understanding the science of mortar rounds and implementing it into improved interior ballistics (IB) models. The long-range goal is improved design and function of the mortar rounds to yield better accuracy and precision.

In the past, lumped parameter IB codes such as IBHVG2 (*1*) have had limited success in simulating mortars due to the complex nature of the firing event. Initiation of the percussion primer ignites the booster charge of black powder pellets. The efflux of the perforated flash tube ignites and initiates flame spread into the tail boom's main propelling charge in the tail boom. After a sufficient pressure is built up inside the tail boom, hot gasses and burning particles are discharged into the mortar launch tube, which may or may not have additional propellant modules. Only at this point does the mortar tube with burning propellant and hot expanding gasses conform somewhat to the conventional ballistic model for which lumped parameter codes were designed.

2. Advancements in IBHVG2

Recent additions to the IBHVG2 code (*2*) allow the modeling of two chambers that contain propellant (rather than the single chamber assumption appropriate for most gun configurations) to represent the mortar configuration. There are two modes of connecting the two chambers—the burst vent mode and the permeable canister mode. In the burst vent mode, the two chambers are separate until the burst pressure is achieved in the inner canister. The burst disk then disintegrates and the two chambers are modeled as one well-stirred reactor with a volume equal to the combined individual volumes of the inner and outer chambers. At this point, the hot gases and any remaining propellant from the inner chamber are assumed to interact instantaneously with any available propellant in the outer chamber and ignite the former outer chamber propellant.

Figure 2 shows a schematic of the burst canister mode. The burst vent mode option is not intended to represent the mortar system; as such, it will not be discussed further in this report.

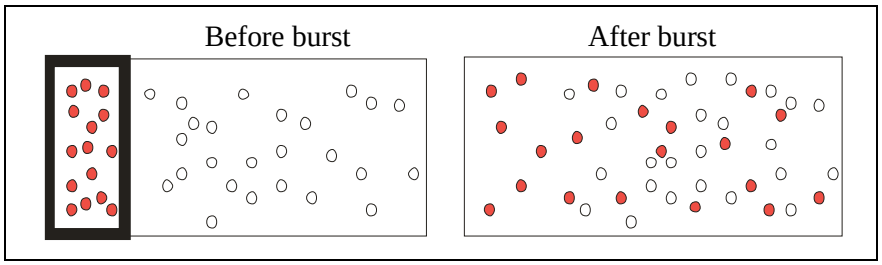

Figure 2. Schematic of the burst canister mode in IBHVG2.

In the permeable canister mode, the inner chamber pressurizes until the burst pressure is achieved, then the impenetrable interface between the two canisters is modeled as a series of holes. This provides a permeable interface allowing gases to flow out of the inner chamber into the outer chamber. If at some point, the gas pressure in the outer chamber exceeds the pressure in the inner chamber, the model allows gas to flow back into the inner chamber. Hot burning particles may flow from the inner to the outer chamber if the particles are small enough to travel through the holes, and the solid discharge coefficient is set to a nonzero value. (Note that the solid discharge coefficient will be discussed in detail later.) Particles are not allowed to travel from the outer canister to the inner canister in this model. Only gas can travel back into the inner chamber. The chambers are both modeled as two distinct, well-stirred reactors with a permeable connection. The burning rate in the chambers is computed using the space mean pressure. Because the two chambers are independent, the pressures may be different, allowing different burning rates in the two chambers.

3. Mortar IB Representation Using HILO

There is a high-pressure canister which represents the tail boom and a low-pressure chamber which represents the mortar tube exterior to the tail boom. This high-low (HILO) feature has proved useful to the lumped parameter IB modeling of mortars. The HILO feature in IBHVG2 was used to model an Army mortar round (a generic representation based on the M934A1) with zero to four exterior propellant modules (referred to as charges, zones, increments, or horseshoes) and the resulting mortar tube. The simulated internal canister (the tail boom) pressure vs. time curve was compared to available experimental data (*3*). In addition to the classical lumped parameter inputs, the HILO option included two new user-defined parameters (essential discharge coefficients)—one which influences the rate of mass of hot gasses that exits the tail boom into the mortar tube and the other which influences the amount of solid burning particles entrained in the hot gases as they emerge from the tail boom.

The data available for input into lumped parameter codes vary widely in reliability. Certain data such as volume can be measured directly, but other data such as burning rate are often less readily available. A sensitivity study on the impact of nine of the input variables on peak pressure and projectile exit velocity was performed on the high and low canister over a range of ~5% the nominal value. The uncertainty of the two new free parameters necessitated a wider range of investigation.

Lumped parameter models are capable of simulating some key mortar variables. However, as Kuo et al. (*3*) point out, mortar firings exhibit significant pressure waves due, in part, to the nonuniform discharge of combustion products from the flash tube. May and Horst (*4*) demonstrate the complexities involved in attempting to eliminate the occurrence of pressure waves. The mortar IB cycle is not only time dependant, but also very spatially complex, many features of which are clearly outside the purview of a lumped parameter or even a one-dimensional (1-D) multiphase flow IB model.

The first stage in the modification of the Army's multidimensional IB code ARL-NGEN3 (*5*–*8*) for mortar simulations is discussed at the end of this report. These modifications are based on successful work in small-caliber simulations using the ARL-NGEN3 code (*9*, *10*).

4. Sensitivity Studies

The IBHVG2 code provides a simple but useful lumped parameter representation of the interior ballistic cycle, embodying such assumptions as uniform and simultaneous ignition of the entire propellant charge, with combustion assumed to take place in a smoothly varying, well-mixed reactor. The burn rate is determined by the instantaneous, space-mean chamber pressure. An assumed, longitudinal pressure gradient is superimposed on the solution at each instant in time to appropriately reduce the pressure on the base of the projectile.

Certain physical parameters used in lumped parameter codes (e.g., burning rate coefficient or exponent) are difficult to measure. As a result, they are often used as adjustable constants (*11*) to fine tune code results to match experimental gun firing data. The effect of data accuracy on IBHVG2 predictions is demonstrated by a series of sensitivity plots. (The current authors are unaware of any published sensitivity plots for IBHVG2 utilizing the two chambers of the HILO option to model a nominal mortar gun system.) This report will focus on propellant-related inputs such as charge weight, propellant force (or impetus; see equation 1), grain diameter, burning rate coefficient (the 'a' in equation 2), burning rate exponent ('n' in equation 2), and covolume of the product gases. The covolume of a gas is a constant in the Noble-Abel equation of state ('b' in equation 3), which represents the volume taken up by the gas molecules in the gas. The covolume becomes important at high (gun) pressures.

$$F \equiv R'T_f \ , \tag{1}$$

where F is the force, R' is ideal gas constant divided by the mean molecular weight of the product gases, and T_f is the adiabatic flame temperature of the propellant.

$$\frac{dm}{dt} = aP^n \rho S \ , \tag{2}$$

where dm/dt is the rate of mass production of propellant gas from burning of the solid propellant, a is the burning rate coefficient, P is pressure, n is the burning rate exponent, ρ is the density of the propellant, and S is the surface area.

$$P\left(V - mb\right) = mR'T \ , \tag{3}$$

where V is the volume, m is the mass of the gas, b is the covolume, and T is temperature of the gas.

In addition, the sensitivity of the two new adjustable parameters in IBHVG2, the Gas Discharge CoeFficient (GDCF; 'g' in equation 4) and the Solid Discharge CoeFficient (SDCF), are investigated. Because they are new parameters, they are investigated over a wider range of values. The pressure differential between the two chambers influences how much combustion gas is transferred from one canister to the other. A complete description of the phenomena which underlies equation 4 can be found in Anderson (*2*). Since IBHVG2 utilizes a well-stirred batch reactor model, the underlying assumption is that the propellant and gas are uniformly distributed in the chamber. This implies that the particles are evenly distributed inside the fluid and that the exiting gas should contain a fraction of propellant particles equivalent to the mass of the exiting gas divided by the total mass of gas in the inner chamber. However, the phenomena of particle slip (i.e., due to inertia of the particles, their motion "slips" behind the gas as it exits the high pressure chamber through the orifices) is accounted for by the introduction of the SDCF. A value of zero indicates that no particles are allowed to exit the inner chamber; a value of unity indicates that the idealized limit of particles are allowed to exit into the main chamber.

$$\frac{dm}{dt} = gP_{out}AM_e\sqrt{\frac{\gamma}{F}} \ , \tag{4}$$

where m is the mass of gas emitted through the tail boom, g is the GDCF, P_{out} is the pressure of the low pressure canister, A is the total area of the openings between the inner and outer canisters, M_e is the Mach number of the exiting gas, γ is the ratio of heat capacities of the gas, F is force, and t is time.

4.1 Pressure-Time Profiles From IBHVG2

Figure 3a displays the simulated pressure-time profiles for the main chamber of a generic 120-mm mortar qualitatively representing the M934A1 round. Shown are five curves varying in the

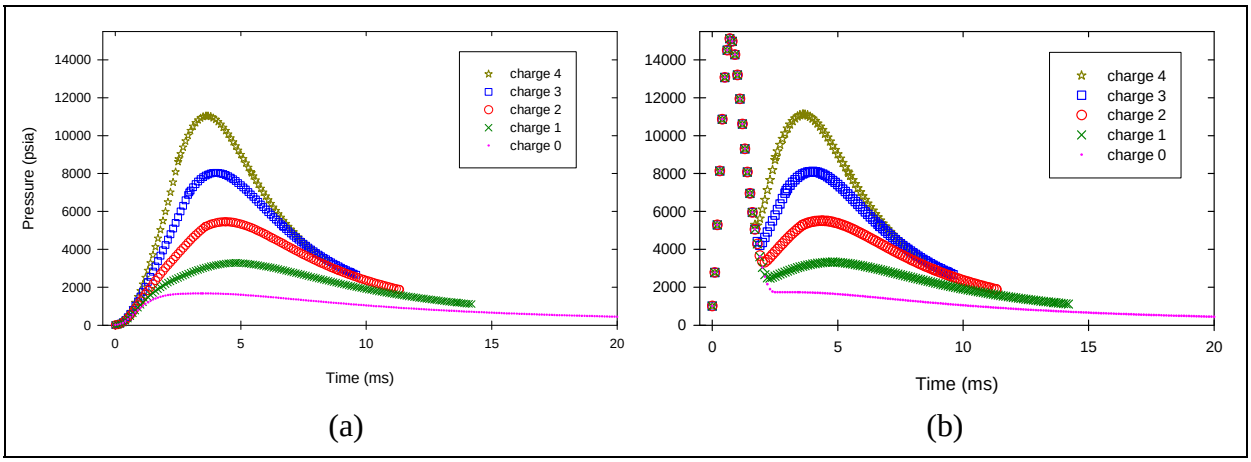

Figure 3. Simulated pressure time profiles of the (a) main chamber and (b) inner chamber for zones 0–4.

number of charges or zones attached to the tail boom of the mortar. (The term "peak pressure" is used to mean peak pressure of the outer or main chamber unless otherwise specified.) The peak pressure is a monotonic function of the number of charges attached to the mortar—the more charges, the higher the peak pressure.

Figure 3b shows the simulated pressure-time curve for the inner chamber of a nominal 120-mm mortar. Shown are five curves varying in the number of charges attached to the tail boom of the mortar. The peak pressures of the inner chamber are independent of the presence of charges in the outer chamber. Because the inner chamber is smaller and pressurizes rapidly, the propellant burns at a faster rate. The inner peak pressure indicates the point in time at which the increase in gas production caused by the increasing pressure is offset by the amount of hot gases and solid propellant particles escaping into the outer chamber. The peak pressure of the inner chamber agrees reasonably with the measurements of Kuo et al. (*3*).

The time series of events as they occur in the simulations follow: ignition and burning of the inner chamber fuel; bursting of the membrane which separates the inner and outer chambers; and discharge of hot gases and particles into the outer chamber, pressurizing the outer chamber and leading to combustion of the propellant therein. Events in the first two steps are independent of conditions in the outer chamber. Only when the pressure in the outer chamber rises to the point where it substantially affects the rate of discharge from the higher pressure chamber into the outer chamber do the inner chamber curves for the different loading conditions begin to deviate. The greater number of charges in the outer chamber, the larger the burning surface and the greater the gasification rate, raising the pressurization rate and concomitantly the burning rate in a bootstrapping fashion. Hence, the outer chamber pressure-time curves diverge accordingly. The latter portion of the inner chamber pressure profiles (i.e., second peaks) simply reflects the overall pressure in the combined chamber volumes.

Figure 4 is an overlay of the inner and outer chamber pressures for charges 2 and 4. The overlap of the inner pressure curves can be readily seen as well as the transition of the inner pressure to the outer pressure when the pressure of the much larger outer chamber approaches the inner chamber.

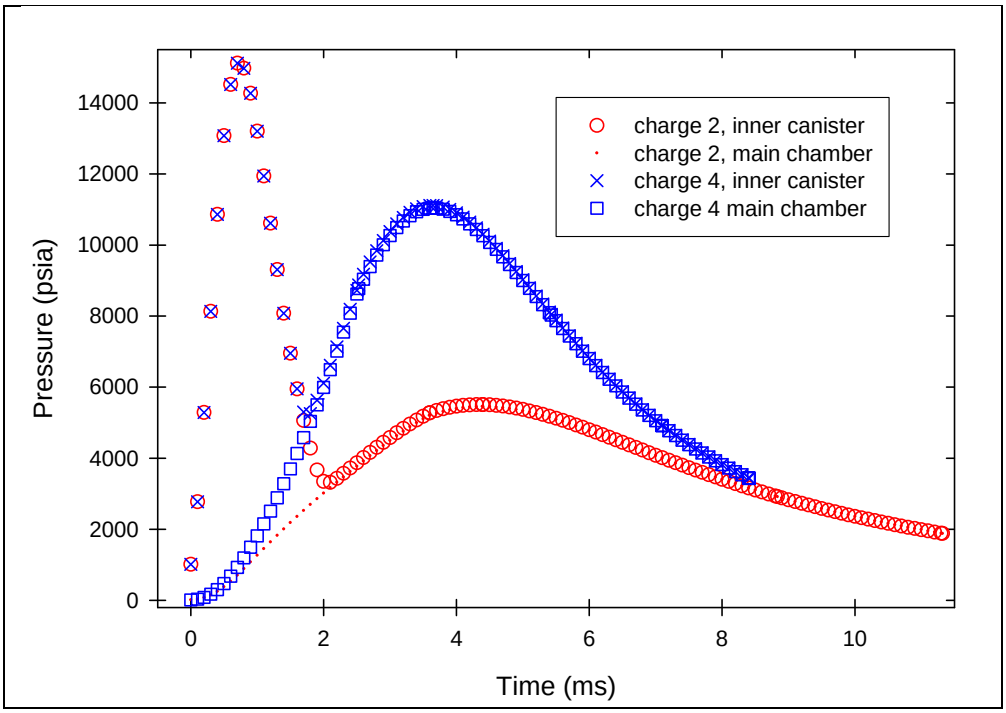

Figure 4. Simulated pressure time profiles of the main and inner chamber for zones 2 and 4.

4.2 Sensitivity of Charge Weight

Turning to the sensitivity runs, the somewhat straightforward results for the sensitivities of predicted peak outer chamber pressure and projectile exit velocity to small changes in propellant charge weight are discussed next. Figure 5a shows the response of peak pressure to small changes in the propellant charge weight for zero, two, and four outer increments, or zones, with separate curves shown for changes in inner and outer chamber charge weights. The charge weight is varied independently in the inner and outer chambers. Not surprisingly, all curves show an increase in peak pressure for increasing charge weight, providing greater initial burning surface and total energy to ultimately pressurize the outer chamber. However, the results become somewhat more interesting upon examination of the individual curves.

Looking first at the impact of changes in charge weight in the inner chamber, the zero-charge case exhibits the largest slope while the four-charge case has the smallest. The slopes monotonically decrease, with an increase in the number of charges, because a given change in the charge weight of the inner canister becomes less of the total charge weight as more external

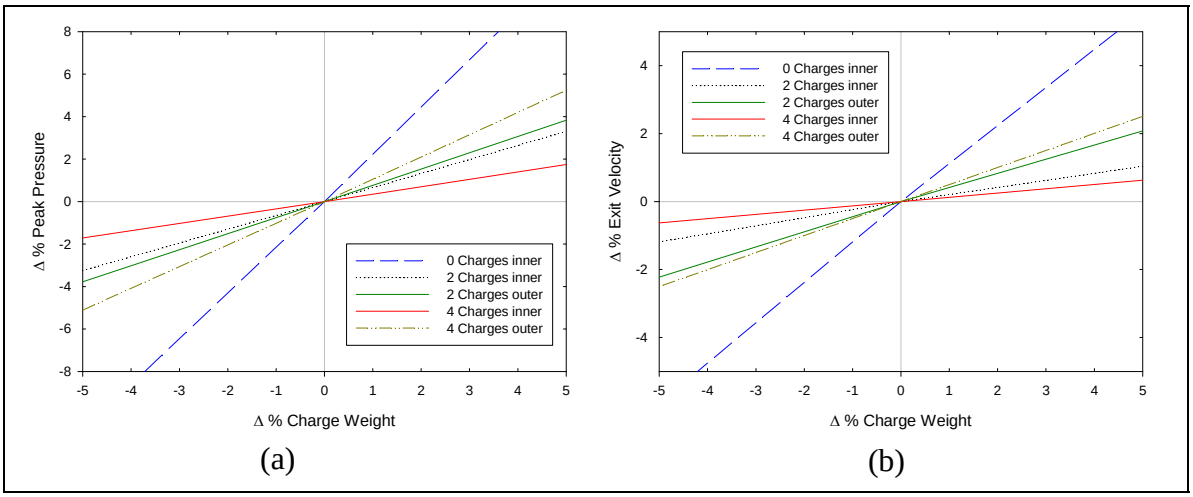

Figure 5. Sensitivity study showing the percent change in the (a) peak pressure of the main chamber and (b) exit velocity as a function of a change in the propellant charge weight for the 120-mm mortar (zones 0, 2, and 4).

charges are included. Comparing similar results for variations in the charge weight in the outer chamber, the four-charge case has the largest slope while the two-charge case has the smallest. The slopes monotonically increase with the number of charges. A 5% increase in four charges is twice as large as a 5% increase in two charges. As the number of charges is increased, the variation of the outer charge weight is an increasingly larger contributor to the gases produced. In turn, the greater increase produces more gas, raising the pressure and the accompanying burning rate, via the bootstrapping mechanism just described.

Figure 5b shows the response of projectile exit velocity to small changes in the charge weight in the inner and outer chambers, with varying number of zones. Results mimic those for the response of maximum chamber pressure-to-charge weight, though at a somewhat reduced level of sensitivity. All curves show an increase in velocity for increasing charge weight. The increasing slope is due to the fact that an increase in amount of propellant equals an increase in the amount of surface area, giving a boost to the amount of gas being generated and thus increasing the pressure. The velocity is the time integral of the pressure as shown in equation 5.

$$V = \int \frac{A_p P}{m_p} dt \ , \tag{5}$$

where V is the projectile velocity, A_p is the area of the projected projectile base, P is the instantaneous pressure at the base, and m_p is the projectile mass. The detailed explanations for the individual curves directly follow those just provided for the pressure sensitivities. The only difference is the lower overall slopes of the curves, a result of the velocity being an integrated function of the overall pressure profile, which, for any given total charge weight, will be less sensitive to small changes in individual parameters than the instantaneous peak pressure. This behavior will be observed in future results.

4.3 Sensitivity to Force

A second way to look at the sensitivity of predicted performance to small changes in total charge energy is to vary the propellant force F (see equation 1) rather than the charge weight. Figure 6a shows how the peak external chamber pressure responds to a small change in the force F of either the inner or outer chamber propellant, again for a range of charge increments. For cases where there is propellant in both the outer and inner chamber (zones 2 and 4), the force is changed independently in the outer and inner chambers. Note that the propellant used in the inner chamber is not necessarily the same as the propellant used in the outer chamber, necessitating treatment of each propellant force F separately. As with the charge weight sensitivity results, an increase in peak pressure accompanies an increase in propellant force under all charge loading conditions. The increasing slope is due to the fact that the greater the force F at constant T_f, the lower the mean molecular weight (MMW) of the gas. The lower MMW pressurizes the chamber more rapidly, leading to a similar sequence of events as described for increases in charge weight in section 4.2.

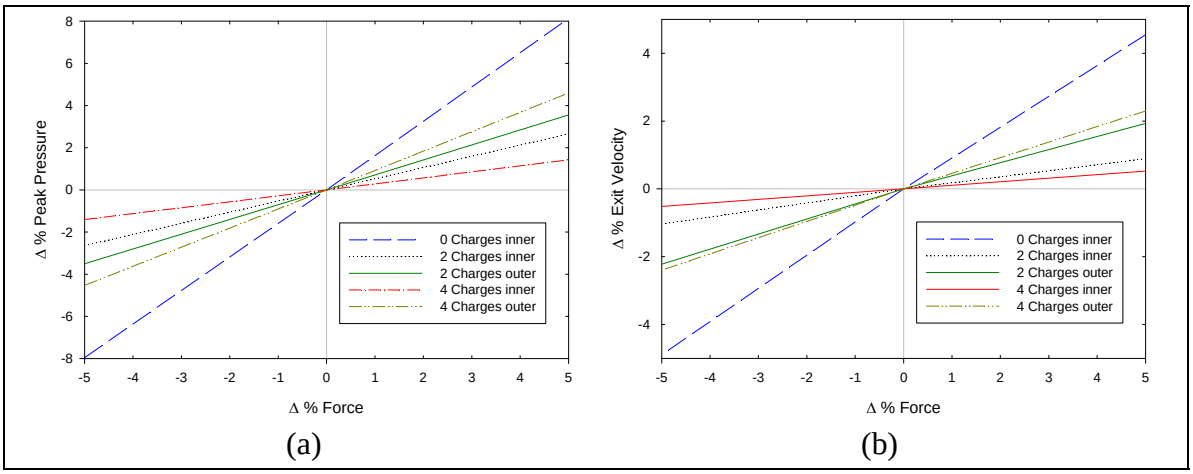

Figure 6. Sensitivity study showing the percent change in the (a) peak pressure of the main chamber and (b) exit velocity as a function of a change in the propellant force for the 120-mm mortar (zones 0, 2, and 4).

Looking first at the impact of the changes in the force of the propellant in the inner chamber, the zero-charge case again has the largest slope while the four-charge case has the smallest. This time, the slopes decrease monotonically with the number of outer chamber charge increments because the variation in the inner propellant force becomes an increasingly smaller contribution to the overall force of the combined charge. Comparing just the changes in the force of the propellant in the outer chamber, the four-charge case has the largest slope while the two-charge case has the smallest. The slopes increase monotonically with the number of charges because the variation in the outer propellant force becomes an increasingly larger contributor to the total force of the combined charge and the bootstrapping effect of pressure on the burning rate just described exacerbates the effect.

Figure 6b shows the response of projectile exit velocity to small changes in the propellant force in the inner and outer chambers with varying number of zones. This situation is completely analogous to that just described for sensitivity of velocity to variations in charge weight; velocity sensitivity curves mimic pressure sensitivity curves but with lower slopes for all conditions for the same reasons. As charge weight and propellant impetus simply provide alternative paths of defining total available propellant charge energy, it is not surprising that the sensitivity results are correspondingly similar.

4.4 Sensitivity to Propellant Diameter

The study of sensitivity to parameters affecting the rate of energy delivery rather than the total quantity of energy delivered will be discussed next. As displayed in equation 2, the rate of gases produced from the burning solid propellant is directly dependent of the area of the burning surface and the rate at which that surface regresses. Even though this study deals with spherical or oblate spherical propellant grains, all classical propellant granulations show that for a given total charge weight, an increase in the major dimension of the grain decreases both the total number of grains in the charge and, more importantly, the available initial burning surface. (Numerous studies have addressed the effects of grain geometry and accompanying progressivity of gas production on gun performance but are not directly relevant to the current study.) Changes in propellant diameters will have an inverse effect on initial burning surface and, hence, initial gas production rates. Also, since propellant dimensions and compositions used in the inner and outer chambers of a mortar are not usually the same, the results here address changes in diameters of the two propellants separately, as was done for charge weights and propellant forces.

Figure 7a displays the response of peak outer chamber pressure to small changes in propellant diameter, with inner and outer chamber propellant changes plotted separately, for various numbers of external chamber charge increments. Consistent with intuition, a decrease in peak pressure accompanies an increase in propellant diameter (hence, a decrease in initial burning surface) under all conditions. Though slopes are negative rather than positive, order of the curves remains the same. Not surprisingly, explanation for these results generally follows the same logic as for previous examples.

Looking first at the impact of changes in the diameter of the propellant in the inner chamber, the zero-charge case has the largest negative slope while the four-charge case has the smallest. The absolute values of the slopes are monotonically decreasing with the number of charges because the overall gas generation is a combination of the gas generated by the propellant in the inner chamber and that generated by the outer chamber propellant. As the number of external charges is increased, the variation of the rate of inner propellant gas generation is an increasingly smaller contribution to the total rate of gas generation. Comparing just the changes in diameter of the propellant in the outer chamber, the four-charge case has the largest negative slope while the two-charge case has the smallest. The slopes are monotonically decreasing with the number of charges, once again, because the overall gas generation depends more and more on the gas production rate of the external charges as the number of increments increases.

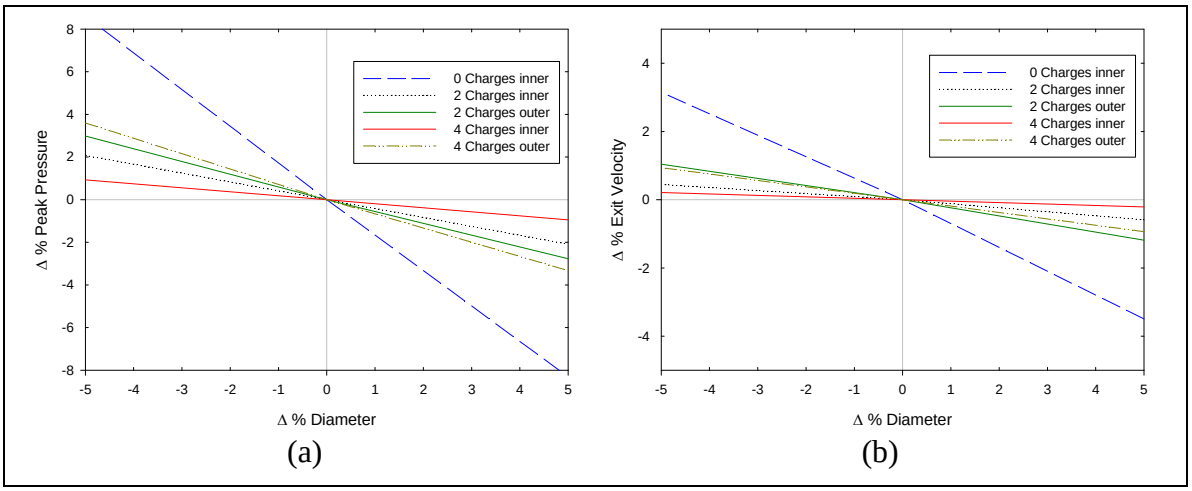

Figure 7. Sensitivity study showing the percent change in the (a) peak pressure and (b) exit velocity as a function of a change in the propellant diameter for the 120-mm mortar (zones 0, 2, and 4).

Figure 7b shows the response of projectile exit velocity to small changes in the propellant diameter for the inner and outer charges varying in the number of zones. All charge variations show a decrease in velocity with increasing diameter, which corresponds to decreasing initial burning surface. Essentially, we see a reduction rather than an increase in gas production rate. However, the situation is analogous to that discussed in section 4.2 except that the reduction in gas production causes a negative slope. Velocity sensitivity curves mimic pressure sensitivity curves, explanations for the ordering of curves remain the same, and slopes are lower for all conditions for the same reasons just described.

4.5 Sensitivity to Burning Rate

Gas production from burning propellant is a direct function of burning surface area and surface regression rate. According to equation 2, the burning (regression) rate can be expressed in terms of the gas pressure raised to an exponent "n" and multiplied by a coefficient "a." This relation implies that the burning rate is also directly dependent on the coefficient "a" itself. Figure 8a shows the response of peak outer chamber pressure to small changes in this burning rate coefficient for each of the two propellants, with various numbers of charges. Figure 8b displays the corresponding results for sensitivity of projectile exit velocity to these same changes in burning rate coefficients and charge increment numbers. Outer and inner burning rate coefficients are changed independently for zones 2 and 4. Results should be completely expected by now, with the ordering of slopes for the curves the same as in previous examples and with the velocity sensitivities similarly lower. Explanations for these results also remain the same, with the slopes decreasing for changes in the inner propellant coefficient as the number of external charges is increased (the change becomes less influential), while the slopes increase for changes in the outer propellant coefficient as the number of charges is increased (the change becomes more influential).

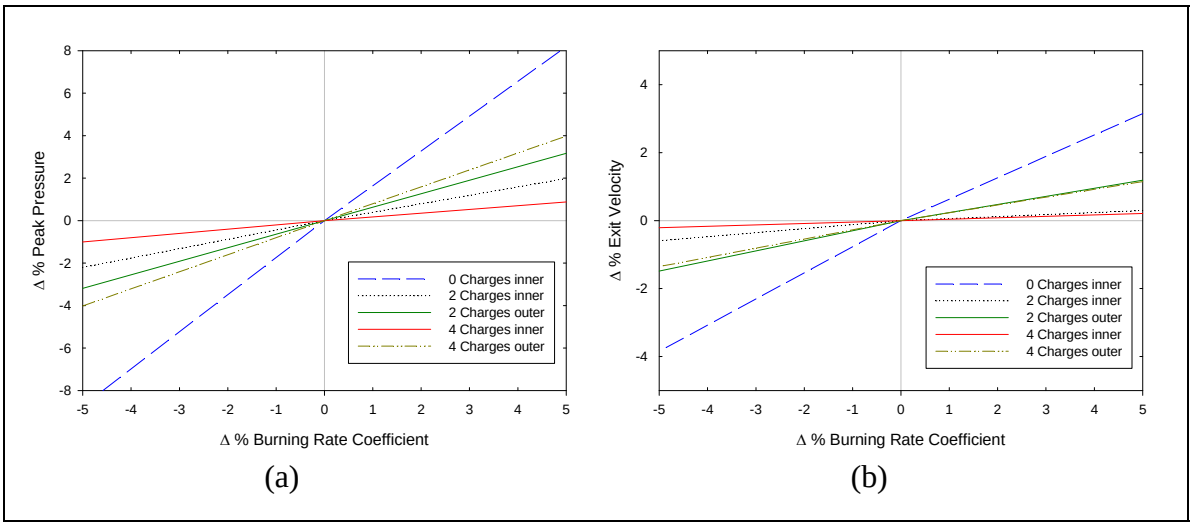

Figure 8. Sensitivity study showing the percent change in the (a) peak pressure of the main chamber and (b) exit velocity as a function of a change in the propellant burning rate coefficient for the 120-mm mortar (zones 0, 2, and 4).

One interesting additional feature should be pointed out about these results. The curves are almost identical, quantitatively and qualitatively to those of figure 7, with the slopes reflected about the x-axis. The explanation is readily found once again in equation 2; gas production rate is directly proportional to burning surface and burning rate coefficient, the former initially being approximately inversely proportional to initial propellant grain. Hence, gas production rate and subsequent peak pressure and velocity should experience inverse responses to initial grain diameter and burning rate coefficient, as evidenced in figures 7 and 8.

The influence of changes in parameters leading to comparable levels of change (e.g., less than a 5% change in pressure and a 2% change in velocity for a 5% variation in the outer chamber propellant at the zone 4 level) has been examined. The influence of a traditionally more influential, and traditionally less known, propellant parameter is examined next as the burning rate exponent "n" in equation 2. Because of its exponential rather than linear influence on the burning rate, very small changes in "n" can be expected to lead to a much greater impact on performance than shown in previous examples. Indeed, figure 9 shows the response of peak pressure and projectile exit velocity to small changes in the burning rate exponents for inner and outer charges, for a various number of outer charge increments. Outer and inner burning rate exponents are changed independently. As expected, all curves show an increase in peak pressure or velocity as the burning rate exponent increases. Indeed, the curves look nearly the same as those for the coefficient variations at first glance. However, note that the both the x-axis and y-axis ranges have been changed and the slopes of the various curves are increased nearly tenfold over those reflecting the coefficient variations in figures 5–8.

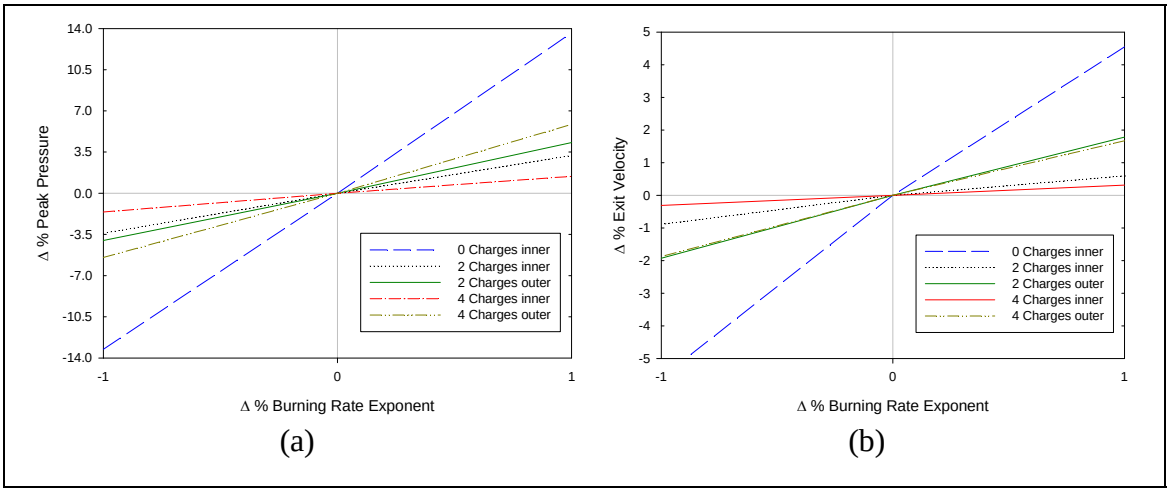

Figure 9. Sensitivity study showing the percent change in the (a) peak pressure of the main chamber and (b) exit velocity as a function of a change in the propellant burning rate exponent for the 120-mm mortar (zones 0, 2, and 4).

Also note that the qualitative nature of the results for pressure and velocity are unchanged. Explanations for these results also remain the same, with the slopes decreasing for changes in the inner propellant coefficient as the number of external charges is increased (the change becomes less influential), while the slopes increase for changes in the outer propellant coefficient as the number of charges is increased (the change becomes more influential). Comparing the changes in burning rate exponent in the inner chamber, the zero-charge case has the largest slope while the four-charge case has the smallest.

4.6 Sensitivity to Covolume

Earlier studies (*11*, *12*) have established that small changes in covolume have little effect on overall performance of large guns (e.g., artillery pieces and tanks). It is expected that there would be an even smaller effect on mortar systems because they operate at significantly lower peak pressures. Figure 10 shows the response of peak pressure to small changes in the covolume for zero and two charges. As expected, the changes are minimal. Because the covolume is a function of the propellant burned, the covolume was varied independently in the outer and inner chambers. All curves show an increase in peak pressure for increasing covolume. The increasing slope is due to the fact that increasing the covolume is equivalent to increasing the volume taken up by the gas, which, in turn, increases the pressure.

4.7 Sensitivity to Projectile Weight

Both modelers and ammunition designers are often interested in the affect the projectile weight has on the performance. Figure 11a shows how the peak pressure changes with a small change in the projectile weight. Also shown is the effect of varying the number of charges from four to two to zero. All charge variations show an increase in peak pressure for increasing projectile

weight. The zero-charge case has the smallest slope while the four-charge case has the largest. The slopes are monotonically increasing with the number of charges. The increasing slope is due to the greater force needed to move the heavier projectile.

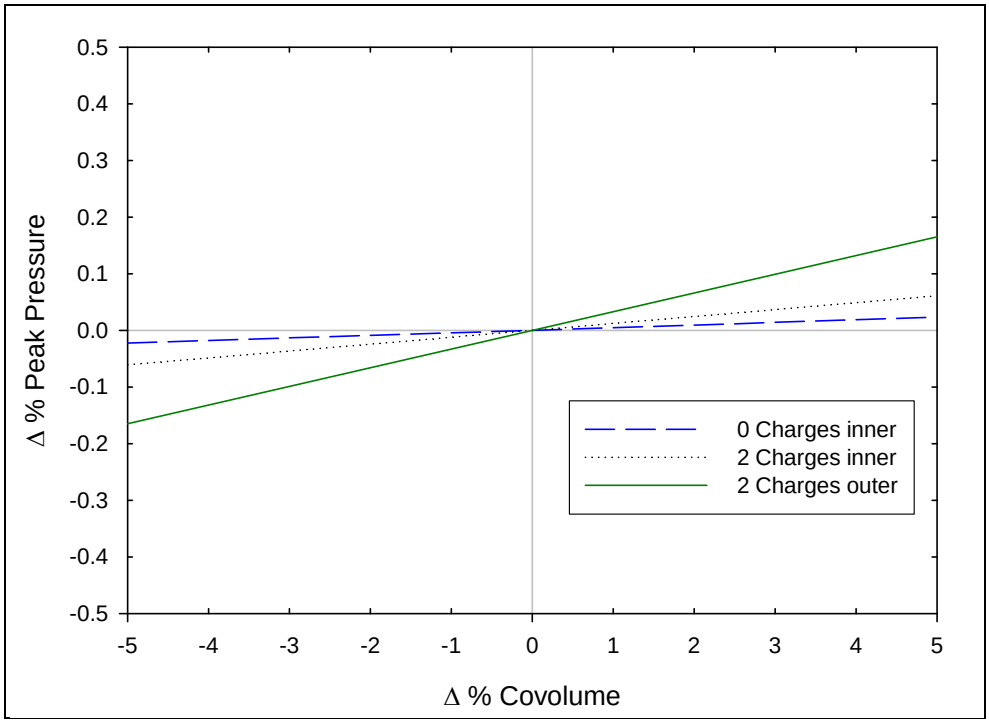

Figure 10. Sensitivity study showing the percent change in the peak pressure of the main chamber as a function of a change in the propellant covolume for the 120-mm mortar (zones 0, 2, and 4).

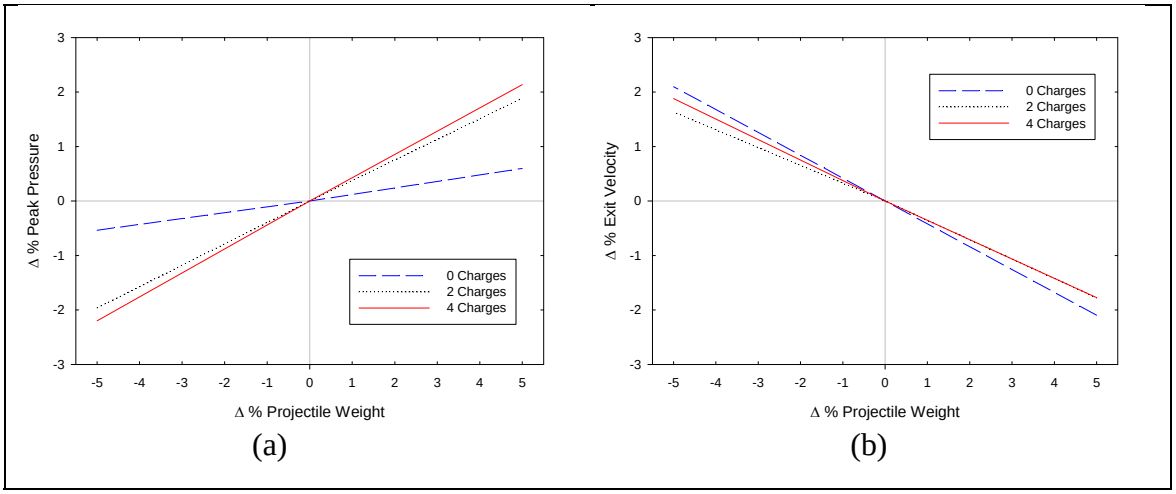

Figure 11. Sensitivity study showing the percent change in the (a) peak pressure of the main chamber and (b) exit velocity as a function of a change in the projectile weight for the 120-mm mortar (zones 0, 2, and 4).

Figure 11b shows how the exit velocity changes with a small change in the projectile weight and varying the number of charges. All charge variations show a decrease in velocity for increasing projectile weight. The zero-charge case has the greatest incline while the four-charge case has the least. This is due to the fact that more propellant charges produce more gas in the same amount of time.

5. Sensitivity Studies of GDCF and SDCF

Two new inputs unique to the HILO version of IBHVG2, for which no previous studies exist, will be studied next. Gas is initially confined to the inner chamber until a preset condition is met, such as the burst pressure for a disk or liner preventing escape of gases prior to rupture. As defined in equation 4, the GDCF influences the rate at which gas exits the inner canister to the outer canister. A value of zero prevents any gas from escaping through the orifices, and a value of unity allows the exit flow to be ideal.

Figure 12 displays the influence of the GDCF on peak pressure and projectile exit velocity predictions for various numbers of external charges. While all charge variations show a decrease in peak pressure for increasing GDCF, data for the zero external charge case exhibit the largest negative slope and those for the four-charge case the smallest. The explanation for this behavior is quite interesting. Pressure builds in the inner chamber because gas is created at a faster rate than it can exit to the outer chamber through the orifices. An increase in the GDCF allows a higher gas discharge rate, resulting in a lower pressure within the high pressure chamber and reducing the rate at which further gases are produced within that chamber. When no charge increments are present in the outer chamber, pressurization in this region results solely from gases ejected from the inner chamber. Increasing the GDCF by lowering internal chamber pressure actually reduces gas production and, via equation 4, subsequent gas discharge as well. This leads not only to a reduction in outer chamber peak pressure but with a greater relative influence (as evidenced by the slope of the curve) than when outer charges are present. In the case where external charges are present, combustion of these increments begins when hot gases and particles are expelled from the inner chamber and pressurize the outer chamber. In the code, combustion in this region is then driven by pressure (recall equation 2), so the greater the amount of gases emitted to the outer chamber, the greater the combustion rate of the outer charges. However, as the number of charges is increased, the influence of the GDCF becomes increasingly smaller because there is increasingly more propellant burning to pressurize the outer chamber. Velocity sensitivities mimic the pressure sensitivity curves but with reduced slopes for the same reasons previously described in section 4.2.

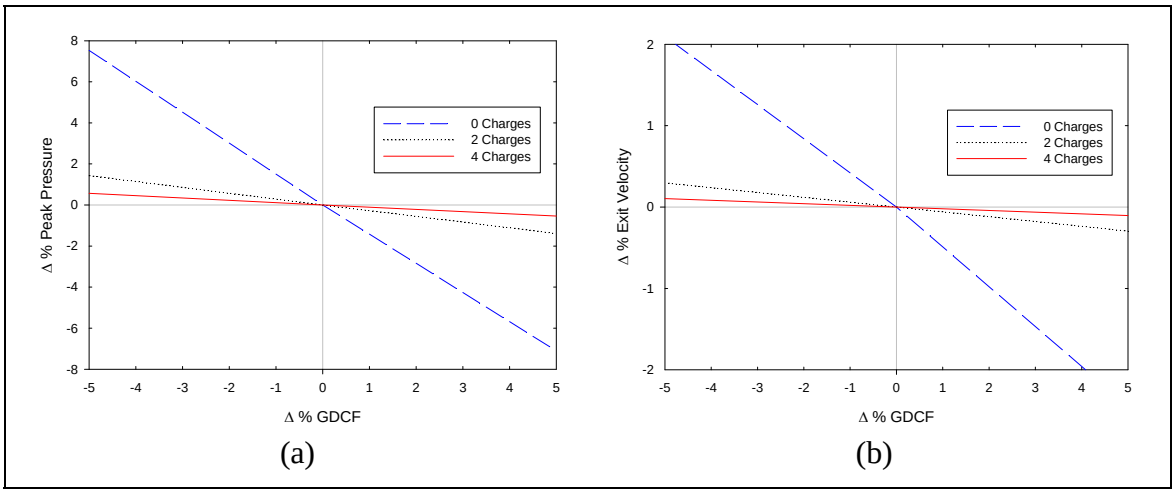

Figure 12. Sensitivity study showing the percent change in the (a) peak pressure of the main chamber and (b) exit velocity as a function of a change in the GDCF for the 120-mm mortar (zones 0, 2, and 4).

As described earlier, the SDCF influences the rate at which solid particles of propellant exit the inner chamber to the outer chamber. As with the inner chamber gas products, solid propellant particles are restrained from exiting the inner chamber until a pressure is reached that initiates the bursting of a membrane. In addition, particles are restrained from exiting the inner chamber if their diameters are too large to fit through its exit ports. The gas-particle mixture is assumed to be well stirred, so the maximum number of particles which can exit the inner chamber is directly proportional to the gas mass fraction leaving through the port holes times the total propellant particles in the inner chamber. The actual number of propellant particles released is then equal to this theoretical maximum times the SDCF. Hence, no particles exit when the SDCF is 0, and a theoretically maximum number of particles exit when the value is unity, provided the particles will fit through the port holes. Note that the current implementation of the HILO routine in IBHVG2 only allows particles to pass from the inner chamber to the outer chamber, not the reverse.

Figure 13 displays the influence of the SDCF on peak pressure and projectile exit velocity, with various numbers of external charges. As with the GDCF results, all charge variations show a decrease in peak pressure and projectile exit velocity with increasing SDCF. Also, the zero external charge case produces the largest negative slopes while the four-charge case has the smallest. There are two slightly different contributors to the observed effect. First, as more particles are discharged into the external chamber, fewer particles remain in the high-pressure chamber to burn and pressurize that region and contribute to the mechanism cited for the GDCF effect. Second, the ejected particles now burn at the lower external chamber pressure, contributing directly to mass generation in that region but at a lower combustion rate. The net result appears to be that sensitivity of performance to the SDCF is similar though slightly lower than to the GDCF.

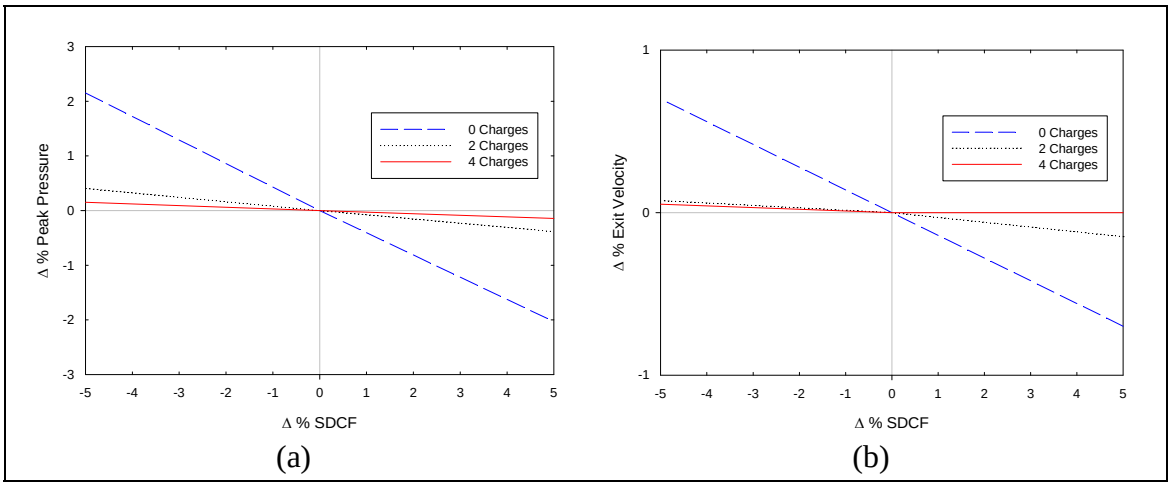

Figure 13. Sensitivity study showing the percent change in (a) peak pressure of the main chamber and (b) exit velocity as a function of a change in the SDCF for the 120-mm mortar (zones 0, 2, and 4).

The GDCFs and SDCFs are new additions to IBHVG2 and deserve additional scrutiny. Beginning with the GDCF, there are two limiting values. The first is the case where the GDCF approaches zero. In the actual limit, there are no hot gases escaping from the inner chamber and, hence, no possibility of the outer chamber being pressurized to accelerate the mortar projectile. However, as the GDCF is increased from zero, gases begin to escape and pressurize the outer chamber, dictating a positive slope for the GDCF sensitivity curve in this region. The second limit occurs when the GDCF is so large that amount of gas leaving the inner chamber leads to equal pressures in both chambers, converting the system from a high-low gun to essentially a single-chamber gun with two propellants. As such, the gun performance loses dependence on the GDCF, and the slope of the sensitivity curve necessarily approaches 0.

Consider now how the SDCF impacts this picture. The SDCF is added to account for the slip, or relative inertia, of the solid and the gas. In the ideal case of a well-stirred reactor with very fine propellant grains, the SDCF would be equal to one, suggesting that variations in the SDCF would not change the expected physics as previously described. Indeed, figure 14, which displays sensitivity results for the zone 2 (i.e., two external charges) configuration, confirms the qualitative similarity of this behavior at the two extreme values of the SDCF. The sensitivity of peak pressure to changes in the GDCF with the SDCF set to 0.1 is shown in figure 14a. Results from the same computations but with the SDCF set to 0.9 are shown in figure 14b. While transition levels differ somewhat, significant physical trends are the same—the slope is positive for very small levels of the GDCF, it transitions through a 0 slope to a negative slope for a range in increasing SCDF values, and finally approaches 0 slope once again as the GDCF approaches unity.

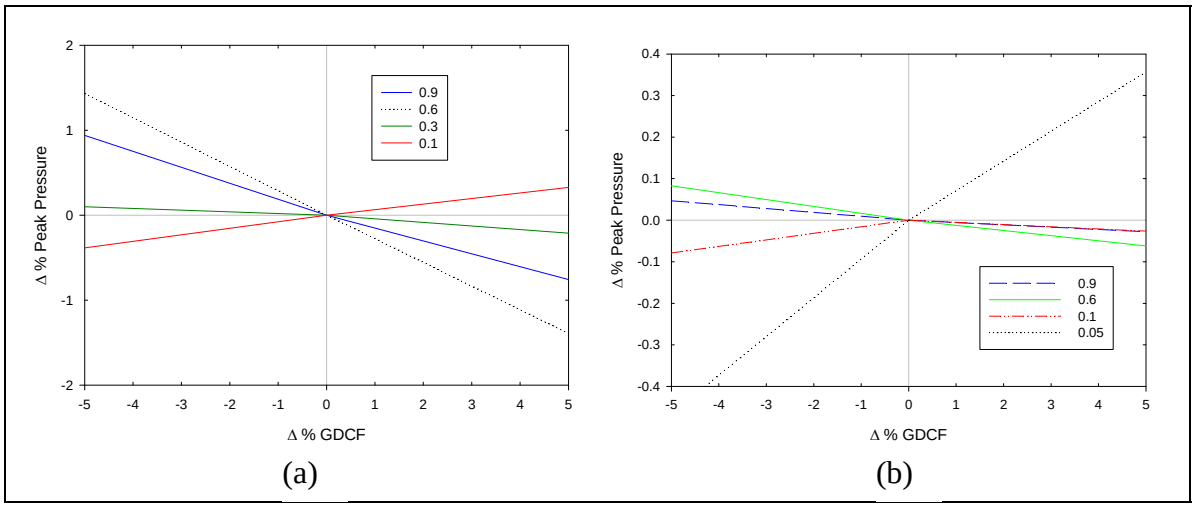

Figure 14. Sensitivity study showing the percent change in the peak pressure of the main chamber as a function of a small change in the GDCF for varying GDCF with the SDCF (a) close to 0.1 and (b) close to 0.9 for the 120-mm mortar zone 2. The GDCF = 0.1 curve in (b) shows that there is a local maxima in the peak pressure.

The influence of these two new input parameters and their interactions are seen to be subtle and significant. Local maxima are observed at which either increases or decreases in the values of the GDCF are seen to lead to a reduction in pressure, an effect not observed with any of the other parameters studied. With predicted gun performance no longer a simple monotonic function of this parameter, the modeler must employ it with considerable care, lest the values of GDCF and SDCF successfully employed for one specific case be found to yield erroneous results under different conditions. The local maxima discovered here may result in predicting the wrong trend in pressure which, in turn, could be catastrophic. Experimental measurements of these parameters would help in bracketing the range of applicability.

A useful sensitivity diagram is provided in figure 15a which shows the relative importance of the parameters investigated for zone 0 on peak pressure. Note that the covolume was omitted because the slightly increasing value was barely noticeable at this scale. Note that in figure 15a, the slope of the sensitivity of diameter is negative, while the slope of the sensitivity of the charge weight is positive. (See figure 10 for covolume sensitivity.) Comparison with Horst and Haukland (*12*) (see figure 15b) shows similar trends in force F, burning rate exponent, and burning rate coefficient.

Figure 16a shows a similar comparison of the parameters investigated for zone 0 on exit velocity. Note the slope of the diameter curve is negative, while the slope of the force curve is positive. Comparison of figure 16a with Horst and Haukland (*12*) (see figure 16b) and others (*11*) shows similar trends.

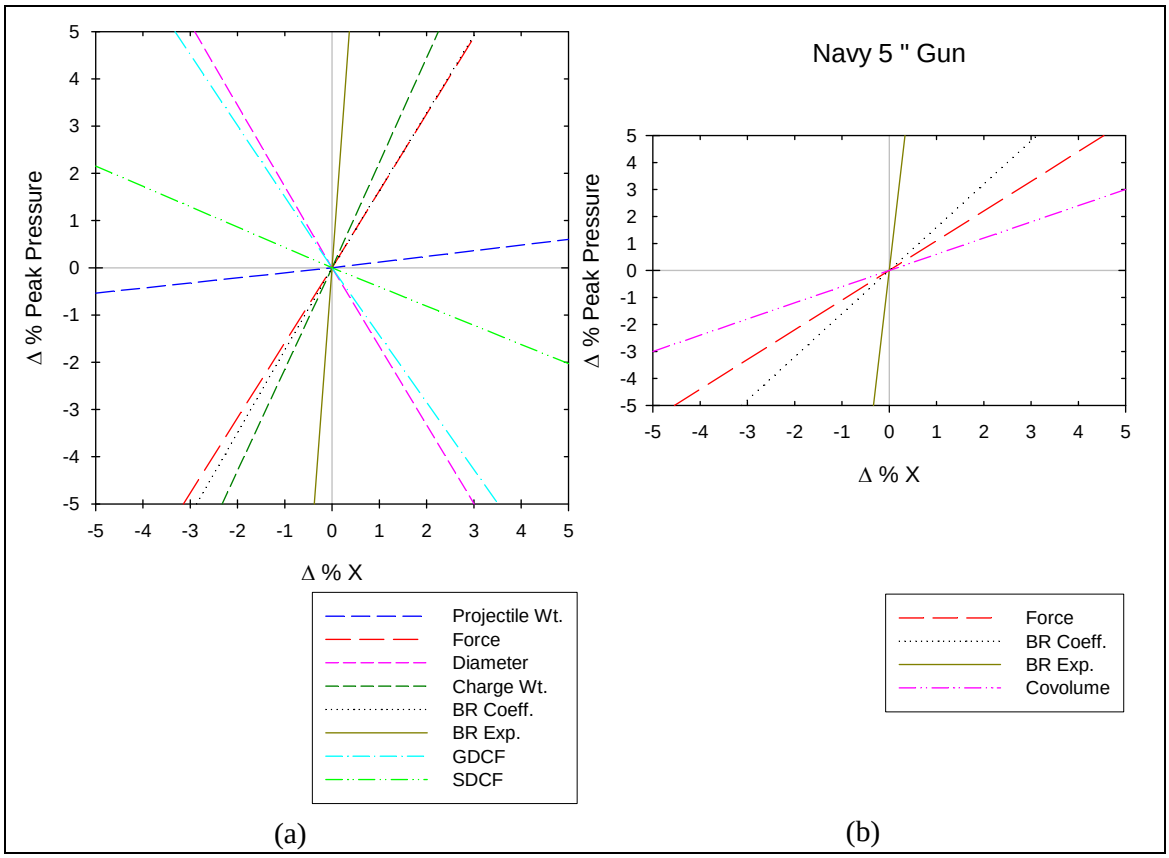

Source: Horst and Haukland (*12*).

Figure 15. (a) Comparison of the relative importance of the percent change in the peak pressure of the main chamber as a function of projectile weight, force, diameter, charge weight, burning rate coefficient and exponent, GDCF, and SDCF for the 120-mm mortar zone 0. (b) Comparison of the relative importance of the percent change in the peak pressure as a function of force, burning rate coefficient and exponent, and covolume from a 1-D IB model representing the Navy 5-in, 54-cal. gun.

6. Progress Toward a Multidimensional Representation

Work has begun to develop a multidimensional interior ballistics code for the mortar that includes modeling of the primer, the energetics within the tailboom, and the mortar propellant increments. The basis of this new model is the current state-of-the-art ARL-NGEN3 IB code (*5–10*).

The Army's NGEN3 code is a multidimensional, multiphase CFD code that incorporates three-dimensional continuum equations along with auxiliary relations into a modular code structure. The components of the interior ballistic flow are represented by the balance equations for a

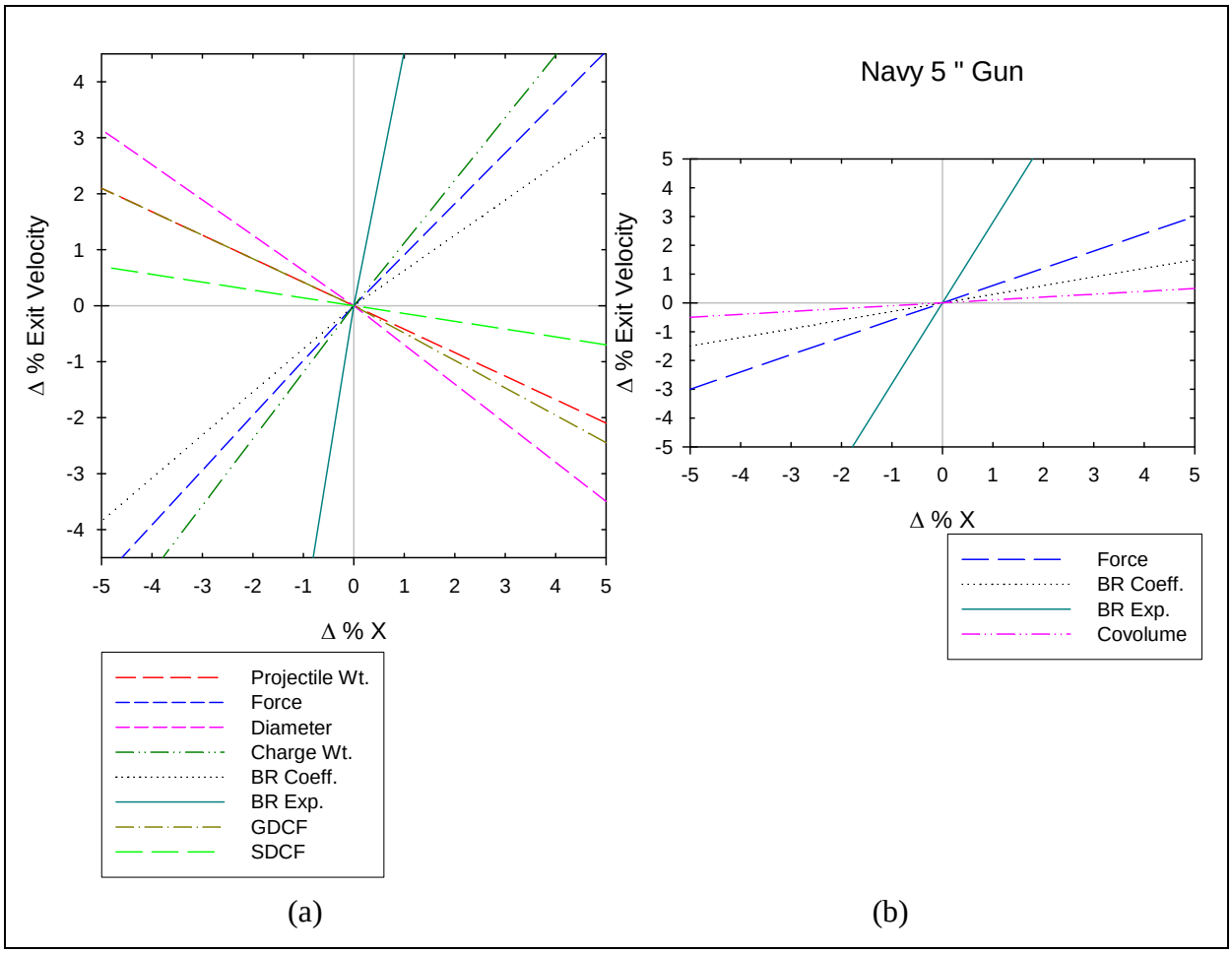

Source: Horst and Haukland (*12*).

Figure 16. (a) Comparison of the relative importance of the percent change in the exit velocity as a function of projectile weight, force, diameter, charge weight, burning rate coefficient and exponent, GDCF, and SDCF for the 120-mm mortar zone 0. (b) Comparison of the relative importance of the percent change in the exit velocity as a function of force, burning rate coefficient and exponent, and covolume from a 1-D IB model representing the Navy 5-in, 54-cal. gun.

multicomponent reacting mixture describing the conservation of mass, momentum, and energy. The numerical representation of these equations as well as the numerical solution thereof is based on a finite-volume discretization and high-order accurate, conservative numerical solution schemes. The spatial values of the dependent variables at each time step are determined by a numerical integration method denoted the continuum flow solver (CFS), which treats the continuous phase and certain discrete phases in a Eulerian fashion. The discrete phases are treated by a Lagrangian formulation, denoted the large particle integrator (LPI), which tracks the particles explicitly and smoothes discontinuities associated with boundaries between propellants yielding a continuous distribution of porosity over the entire domain. The manner of coupling between the CFS and the LPI is through the attribution of appropriate propellant properties. The

solid propellant is modeled using Lagrange particles that regress, produce combustion product gases, and respond to gas-dynamic and physical forces. Individual grains are not resolved; rather, propellant is distributed within specified regions in the gun chamber. The constitutive laws that describe interphase drag, form-function, etc., determine preferred gas flow paths through these regions and responses of the propellant to gas-dynamic forces. Regions encased in impermeable boundaries only yielding to gas-dynamic flow after a prescribed pressure load is reached act as rigid bodies within the gun chamber. Using computational particles to represent the propellant charge permits a host of modeling features that enhances the representation of charge details.

Figure 17 shows a schematic of the computational domain proposed in the ARL-NGEN3 code for simulation of the 120-mm mortar. Note that in this figure, the ordinate is magnified by about a factor of 10. In the axial direction, the domain extends from the breech face (X = 0) to the base of the projectile at 47 cm (i.e., defined for the present application as the location on the projectile where the diameter matches the launch tube). Since, for this case, an axisymmetric configuration is assumed, the domain extends in the radial from the centerline to the radial wall of the mortar tube (6-cm radius) and the fin set (positioned on the tailboom from about 0 to 5 cm) is excluded. For the ARL-NGEN3 code, the tail boom of the mortar (i.e., region extending axially from the tube wall to 21 cm, with a radius of 2.1 cm), while joined to the afterbody of the mortar, is nonetheless modeled as part of the overall propelling charge and ignition mechanism, with explicit treatment of the internal tail boom components.

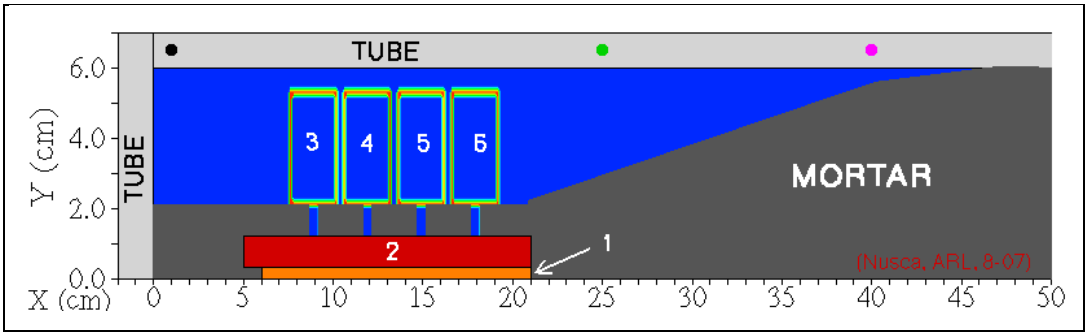

Figure 17. ARL-NGEN3 code setup for mortar simulation.

Several regions of charge and/or ignition stimuli are identified in the figure. Region 1, which extends along the centerline from 6 to 21 cm and within the tail boom, represents the innermost tube of the igniter (radius of 0.32 cm). In the actual mortar, this region, which contains the primer and five pellets of black powder (BP), is otherwise empty. An array of radial holes vents primer, burning BP, and other gases into region 2. In the model, this region is occupied by an igniter mass flow table that essentially generates an even spatial distribution of hot gases from burning BP (1 g) that is fully ignited at time zero and burns for 2 ms. Region 2 is occupied with

60 g of M48 (undeterred ball propellant) which is distributed along the length of the inner tube from 5 to 21 cm and extends radially from 0.32 to 1.2 cm (i.e., diameter of 2.4 cm around the inner tube of 0.64-cm diameter). This region of propellant is directly exposed to region 1; there is no consideration of a physical radial barrier between regions 1 and 2. Regions 3–6 are four axisymmetric charges, each containing 115 g of M47 propellant. Note that M47 is a deterred ball propellant consisting of a core and a surface coating that have distinct burn rate properties included in the model. The diameter of the M47 propellant grain is about half of the M48 propellant. Regions 2–6 are separated by a solid section of the tailboom perforated with four radial strips at the outer radius (2.1 cm) and beneath each of the four charges.

ARL-NGEN3 code models each of the regions of ball propellant (i.e., regions 2–6) explicitly using an array of Lagrange particles that are initially ordered within the boundaries of each region but are free to move according to the appropriate governing equations as the simulation proceeds. Each LPI particle has the same size consideration, thermodynamic, mass, and burning properties as the propellant it represents. The walls of the tail boom (i.e., enclosing regions 1 and 2) are solid regions in the model and managed by internal boundary condition routines. The walls of each charge module (i.e., regions 3–6) are composed of combustible case material (about 2300 J/g) with distinct thermodynamic, mass, and burning parameters. These walls, which are also represented by special Lagrange particles, remain impermeable (which also means the charges act as rigid bodies) until a specified wall overpressure is reached or a wall burn-through condition is realized. Yielding of the charge walls is spatially resolved in the model. Nominal overpressure burst criterion was utilized; however, there is a future requirement for a modeling sensitivity study involving this parameter.

The paper by Schmidt et al. (*13*) was the first to address the modeling configuration of figure 17, which produced intriguing results. However, the paper failed to include the propellant region 2; this region was empty space in the simulation. A subsequent paper by Schmidt et al. (*14*) was the first to address the modeling configuration of figure 17 in its entirety.

7. Conclusions

In summary, we exploited the HILO capability in the IBHVG2 lumped-parameter interior ballistic code, to obtain the sensitivity of predicted peak pressures and projectile exit velocities to a range of input parameters associated with the propelling charges for a generic 120-mm mortar. While such studies have been performed in the past on conventional single-chamber guns, the current investigation is believed to represent the first performed on a HILO ballistic system such as the mortar, and in particular, the first time the influence of discharge coefficients between the two chambers has been studied. Sensitivity of performance to classical propelling charge parameters, for both high and low chambers, is consistent with available data for conventional

guns, where available (*11*, *12*). Sensitivity of mortar performance to the gas and solid discharge coefficients was found to be somewhat more complex and showed a local maxima in peak pressure for the first time.

Sensitivity studies such as those reported herein and in the references aid the modeler by identifying the most critical inputs. As with conventional guns, the burning rate exponent was identified as the most critical for the mortar, with the inner charge exponent most significant when no outer charges were present, but the outer charge exponent quickly achieving dominance as the larger, outer chamber increments were added. All other input parameters studied exhibited approximately an order of magnitude lower influence on performance, with their influence being approximately linear over the region of variation studied (except for the discharge coefficients as previously noted). While actual experimental data for input parameters to interior ballistic models are always highly desirable, it is realized that such data are not always available and some inputs are often empirically fit to provide matches to experimental performance. With the GDCF and SDCF inputs, the modeler is cautioned to obtain any such fits over a range of gun conditions before applying them to new conditions with any confidence.

8. References

1. Anderson, R. D.; Fickie, K. D. *IBHVG2 – A User's Guide*; BRL-TR-2829; U.S. Army Ballistics Research Laboratory: Aberdeen Proving Ground, MD, July 1987.

2. Anderson, R. D. *IBHVG2: Mortar Simulation with Interior Propellant Canister*; ARL-TR-3760; U.S. Army Research Laboratory: Aberdeen Proving Ground, MD, March 2006.

3. Kuo, K.; Acharya, R.; Ferrara, P.; Moore, J. Method of Characteristics Simulation of Interior Ballistics Processes of M1020 Ignition cartridge in a 120-mm Mortar System. *Proceedings of the 40th JANNAF Combustion Meeting*, CPIA Publication JSC CD-39, June 2005.

4. May, I. W.; Horst, A. W. Charge Design Considerations and Their Effect on Pressure Waves in Guns. *Interior Ballistics of Guns (Progress in Astronautics and Aeronautics)*; Krier and Summerfield, Eds.; AIAA: New York, NY, 1979; Vol. 66.

5. Gough, P. S. Modeling Arbitrarily Packaged Multi-Increment Solid Propellant Charges of Various Propellant Configurations. *Proceedings of the 33rd JANNAF Combustion Meeting*, CPIA Publication 653, November 1996.

6. Gough, P. S. *Formulation of a Next-Generation Interior Ballistic Code*; ARL-CR-68; U.S. Army Research Laboratory: Aberdeen Proving Ground, MD, September 1993.

7. Nusca, M. J.; Gough, P. S. *Numerical Model of Multiphase Flows Applied to Solid Propellant Combustion in Gun Systems*, AIAA Paper No. 98-3695, July 1998.

8. Nusca, M. J. *High-Performance Computing and Simulation for Advanced Armament Propulsion*; ARL-TR-3215; U.S. Army Research Laboratory: Aberdeen Proving Ground, MD, June 2004.

9. Schmidt, J. R.; Nusca, M. J. *Progress in the Development of a Multiphase Turbulent Model of the Gas/Particle Flow in a Small-Caliber Ammunition Primer*; ARL-TR-3860; U.S. Army Research Laboratory: Aberdeen Proving Ground, MD, August 2006.

10. Schmidt, J. R.; Nusca, M. J. *Investigation of Small-Caliber Primer Function Using Multiphase Computational Model*; ARL-TR-4514; U.S. Army Research Laboratory: Aberdeen Proving Ground, MD, July 2008.

11. Baer, P. G. Practical Interior Ballistic Analysis of Guns. *Interior Ballistics of Guns (Progress in Astronautics and Aeronautics)*; Krier and Summerfield, Eds.; AIAA: New York, NY, 1979; Vol. 66.

12. Horst, A. W.; Haukland, A. C. *Gun Interior Ballistics: 1972 Annual Report*; IHTR 386, U.S. Naval Ordnance Station: Indian Head, MD, April 1973.

13. Schmidt, J. R.; Nusca, M. J.; Horst, A. W. Mortar Interior Ballistics: Sensitivity Studies Using IBHVG2 and Progress Toward a Multi-dimensional Representation. *Proceedings of the 54th JANNAF Propulsion Meeting*, CPIAC, Denver, CO, May 2007.

14. Schmidt, J. R.; Nusca, M. J.; Horst, A. W. Progress Toward a Multi-dimensional Representation of Mortar Interior Ballistics. *Proceedings of the 42nd JANNAF Combustion Meeting*, CPIAC, Boston, MA, May 2008.

NO. OF
COPIES ORGANIZATION

1 (PDF only) DEFENSE TECHNICAL INFORMATION CTR
DTIC OCA
8725 JOHN J KINGMAN RD
STE 0944
FORT BELVOIR VA 22060-6218

1 DIRECTOR
US ARMY RESEARCH LAB
IMNE ALC HRR
2800 POWDER MILL RD
ADELPHI MD 20783-1197

1 DIRECTOR
US ARMY RESEARCH LAB
AMSRD ARL CI OK TL
2800 POWDER MILL RD
ADELPHI MD 20783-1197

1 DIRECTOR
US ARMY RESEARCH LAB
AMSRD ARL CI OK PE
2800 POWDER MILL RD
ADELPHI MD 20783-1197

ABERDEEN PROVING GROUND

1 DIR USARL
AMSRD ARL CI OK TP (BLDG 4600)

NO. OF COPIES ORGANIZATION

3 DIRECTOR
US ARMY RESEARCH LAB
AMSRD ARL RO P
D MANN
R ANTHENIEN
TECH LIB
PO BOX 12211
RESEARCH TRIANGLE PARK NC
27709-2211

8 US ARMY AVIATN & MIS CMND
AMSRD AMR PS PT
W CHEW
C DOLBEER
J LILLY
M LYON
J FISHER
B MARSH
R MICHAELS
D THOMPSON
REDSTONE ARSENAL AL
35898-5249

1 PM MAS
SFAE AMO MAS
M BUTLER
BLDG 354
PICATINNY ARSENAL NJ
07806-5000

1 PM CAS
SFAE AMO CAS
J RUTKOWSKI
BLDG 171M
PICATINNY ARSENAL NJ
07806-5000

8 DIR BENET WEAPONS LAB
M AUDINO
R DILLON
R FISCELLA
R HASENBEIN
E KATHE
K MINER
S SOPOK
J MCNEIL
WATERVLIET NY 12189-4000

1 CDR US ARMY ARDEC
R CARR
BLDG 65N
PICATINNY ARSENAL NJ 07806-5000

NO. OF COPIES ORGANIZATION

6 CDR US ARMY ARDEC
C ADAM
P HUI
S EINSTEIN
J O'REILLY
J SHIN
E CARAVACA
BLDG 382
PICATINNY ARSENAL NJ 07806-5000

1 CDR US ARMY ARDEC
R CIRINCIONE
BLDG 171M
PICATINNY ARSENAL NJ 07806-5000

2 CDR US ARMY ARDEC
J LANNON
B MACHAK
BLDG 1
PICATINNY ARSENAL NJ 07806-5000

1 CDR US ARMY ARDEC
E LOGSDEN
BLDG 65S
PICATINNY ARSENAL NJ 07806-5000

2 CDR US ARMY ARDEC
S NICHOLICH
R SURAPANENI
BLDG 3022
PICATINNY ARSENAL NJ 07806-5000

1 CDR US ARMY ARDEC
P O'REILLY
BLDG 407
PICATINNY ARSENAL NJ 07806-5000

1 CDR US ARMY ARDEC
A SABASTO
BLDG 94
PICATINNY ARSENAL NJ 07806-5000

1 CDR
RADFORD ARMY AMMO PLANT
SMCAR QA HI LIB
RADFORD VA 24141-0298

2 CDR NAVAL RSRCH LAB
TECH LIB
J BORIS
WASHINGTON DC 20375-5000

NO. OF COPIES	ORGANIZATION
4	OFFICE OF NVL RSRCH J GOLDWASSER D SIMONS D ROBERSON P COLOLLY 875 N RANDOLPH ST RM 653 ARLINGTON VA 22203-1927
1	CDR NSWC TECH LIB DAHLGREN VA 22448-5000
3	CDR NAWC A ATWOOD S BLASHILL T PARR CH1NA LAKE CA 93555-6001
1	AIR FORCE RSRCH LAB MNME EN MAT BR B WILSON 2306 PERIMETER RD EGLIN AFB FL 32542-5910
1	AIR FORCE OFC OF SCI RSRCH M BERMAN 875 N RANDOLPH ST STE 235 RM 3112 ARLINGTON VA 22203-1768
1	NASA LANGLEY RSRCH CTR D BUSHNELL MS 110 HAMPTON VA 23681-2199
1	DIR SANDIA NATL LABS M BAER DEPT 1512 PO BOX 5800 ALBUQUERQUE NM 87185
2	DIR LLNL L FRIED M MURPHY PO BOX 808 LIVERMORE CA 94550-0622
1	CENTRAL INTLLGNC AGCY J BACKOFEN RM 4PO7 NHB WASHINGTON DC 20505

NO. OF COPIES	ORGANIZATION
1	BATTELLE EAST SCI & TECH A ELLIS 1204 TECHLGY DR ABERDEEN MD 21001-1228
2	JHU CHEM PROP INFO AGCY W HUFFERD R FRY 10630 LITTLE PATUXENT PKWY STE 202 COLUMBIA MD 21044-3200
1 (CD only)	OUSD (AT&L)/STRAT & TACT SYS MUNITIONS T MELITA 3090 DEFENSE PENTAGON RM 3B1060 WASHINGTON DC 20301-3090
1	BRIGHAM YOUNG UNIV DEPT OF CHEM ENGRG M BECKSTEAD PROVO UT 84601
1	CALIF INST OF TECHLGY F CULICK 204 KARMAN LAB MS 301 46 1201 E CALIFORNIA ST PASADENA CA 91109
2	UNIV OF ILLINOIS DEPT OF MECH INDUST ENGRNG H KRIER R BEDDINI 144 MEB 1206 N GREEN ST URBANA IL 61801-2978
5	PENN STATE UNIV DEPT OF MECHL ENGRG K KUO T LITZINGER G SETTLES S THYNELL V YANG UNIVERSITY PARK PA 16802-7501
1	INST FOR ADVNCD TECHNLGY 3925 W BRAKER LN STE 400 AUSTIN TX 78759-5316

NO. OF
COPIES ORGANIZATION

1 ARROW TECHLGY ASSOC INC
1233 SHELBURNE RD D 8
SOUTH BURLINGTON VT 05403

1 ALLEGHENY BALLISTICS LAB
PO BOX 210
ROCKET CENTER WV 26726

1 ATK ORDNANCE
4700 NATHAN LANE
PLYMOUTH MN 55442

3 ATK AMMO & ENERGETICS
RADFORD ARMY AMMO PLANT
D WORRELL
W WORRELL
S RITCHIE
RT 114 PO BOX 1
RADFORD VA 24141-0299

4 ATK THIOKOL
P BRAITHWAITE
T FARABAUGH
W WALKUP
R WARDLE
PO BOX 707
BRIGHAM CITY UT 84302-0707

1 ATK ELKTON
J HARTWELL
PO BOX 241
ELKTON MD 21921-0241

1 BAE ARMAMENT SYS DIV
J DYVIK
4800 E RIVER RD
MINNEAPOLIS MN 55421-1498

1 GEN DYNAMICS ST MARKS
H RAINES
PO BOX 222
SAINT MARKS FL 32355-0222

1 GEN DYNAMICS ARM SYS
J TALLEY
128 LAKESIDE AVE
BURLINGTON VT 05401

3 VERITAY TECHGY INC
R SALIZONI
J BARNES
E FISHER
4845 MILLERSPORT HWY
EAST AMHERST NY 14501-0305

NO. OF
COPIES ORGANIZATION

2 DIRECTOR
US ARMY RSRCH LAB
IMNE ALC PWO
G BROWN
2800 POWDER MILL RD
ADELPHI MD 20783-1197

ABERDEEN PROVING GROUND

55 DIR USARL
AMSRD ARL WM
B FORCH
P PLOSTINS
AMSRD ARL WM B
M ZOLTOSKI
AMSRD ARL WM BD
W ANDERSON
R BEYER
A BRANT
S BUNTE
C CANDLAND
L CHANG
J COLBURN
P CONROY
B HOMAN
A HORST
S HOWARD
P KASTE
A KOTLAR
R LIEB
K MCNESBY
M MCQUAID
A MIZIOLEK
J MORRIS
J NEWILL
M NUSCA (5 CPS)
R PESCE-RODRIGUEZ
S PIRAINO
B RICE
R SAUSA
E SCHMIDT
J SCHMIDT (4 CPS)
A WILLIAMS
AMSRD ARL WM BA
B DAVIS
D HEPNER (3 CPS)
G KATULKA
D LYON
AMSRD ARL WM BC
G COOPER
J DESPIRITO
F FRESCONI
J GARNER

NO. OF
COPIES ORGANIZATION

B GUIDOS
J SAHU
S SILTON
P WEINACHT
AMSRD ARL WM M
S MCKNIGHT
AMSRD ARL WM SG
T ROSENBERGER
AMSRD ARL WM T
P BAKER
W CIEPIELA